NANO LETTERS

LETTER

pubs.acs.org/NanoLett

Solution-Processed Graphene/MnO_2 Nanostructured Textiles for High-Performance Electrochemical Capacitors

Guihua Yu,[†,¶] Liangbing Hu,[‡,¶] Michael Vosgueritchian,[†] Huiliang Wang,[‡] Xing Xie,[§] James R. McDonough,[‡] Xu Cui,[†] Yi Cui,[*,‡] and Zhenan Bao[*,†]

[†]Department of Chemical Engineering, [‡]Department of Materials Science and Engineering, and [§]Department of Civil and Environmental Engineering, Stanford University, Stanford, California 94305, United States

Supporting Information

ABSTRACT: Large scale energy storage system with low cost, high power, and long cycle life is crucial for addressing the energy problem when connected with renewable energy production. To realize grid-scale applications of the energy storage devices, there remain several key issues including the development of low-cost, high-performance materials that are environmentally friendly and compatible with low-temperature and large-scale processing. In this report, we demonstrate that solution-exfoliated graphene nanosheets (~5 nm thickness) can be conformably coated from solution on three-dimensional, porous textiles support structures for high loading of active electrode materials and to facilitate the access of electrolytes to those materials. With further controlled electrodeposition of pseudocapacitive MnO_2 nanomaterials, the hybrid graphene/MnO_2-based textile yields high-capacitance performance with specific capacitance up to 315 F/g achieved. Moreover, we have successfully fabricated asymmetric electrochemical capacitors with graphene/MnO_2-textile as the positive electrode and single-walled carbon nanotubes (SWNTs)-textile as the negative electrode in an aqueous Na_2SO_4 electrolyte solution. These devices exhibit promising characteristics with a maximum power density of 110 kW/kg, an energy density of 12.5 Wh/kg, and excellent cycling performance of ~95% capacitance retention over 5000 cycles. Such low-cost, high-performance energy textiles based on solution-processed graphene/MnO_2 hierarchical nanostructures offer great promise in large-scale energy storage device applications.

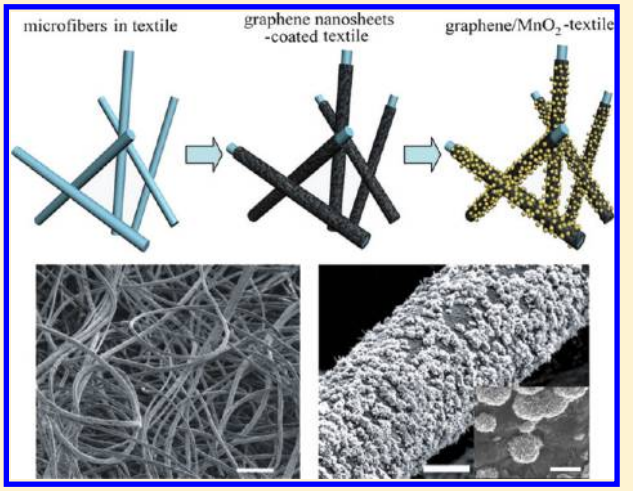

KEYWORDS: electrochemical capacitors, textile, solution process, graphene nanosheets, MnO2

Developing a sustainable and renewable energy future has been one of the most important tasks for scientists and engineers worldwide to address the rapidly increasing global energy consumption coupled with the critical issue of climate change. With increased renewable energy production from solar and wind, efficient energy storage systems are needed to make the best of the electricity generated from these intermittent, renewable sources. Among the various energy storage systems, chemical storage devices (batteries) and electrochemical capacitors (ECs) are two key technological systems that lead the state-of-the-art electrical energy storage systems.[1−3] Batteries have been the technology of choice for many applications; virtually all portable electronics rely on energy stored chemically in them, because they can store large amounts of energy in a lightweight and compact structure and meanwhile provide suitable power levels for certain applications. However, existing battery technologies have performance and cost limitations such as short shelf and cycle life, and relatively slow charging/discharging rates at high power densities. ECs, also known as supercapacitors or ultracapacitors, emerge as a very attractive alternative to batteries and offer a number of potentially high-impact characteristics including high power density (1−2 orders of magnitude higher than that of batteries) fast charging and discharging within seconds (i.e., fast response time), superior cycle lifetime (2−3 orders of magnitude better than that of batteries), and high reliability. ECs have been used in a variety of applications ranging from portable consumer electronics, computer memory backup systems, to hybrid electric vehicles and next-generation all-electric vehicles, and to large industrial scale power and energy management.[4,5]

Depending on the charge storage mechanism as well as the active materials used, ECs can be often distinguished into three types: electric double-layer capacitors (EDLCs), pseudocapacitors, and hybrid electrochemical capacitors. EDLCs, which store charges electrostatically via reversible ion absorption at the electrode/electrolyte interface, commonly use carbon-based active electrode materials with high surface area.[6,7] In contrast,

Received: April 25, 2011

dx.doi.org/10.1021/nl2013828 | *Nano Lett.* XXXX, XXX, 000–000

pseudocapacitors use fast and reversible redox reactions at the surface of the electroactive materials for charge storage. The large specific pseudocapacitance of faradaic electrodes (typically 300−1000 F/g) exceeds that of carbon-based materials using double layer charge storage, resulting in great interest in these systems. Typical active pseudocapacitive materials include transition metal oxides such as RuO_2, Fe_3O_4, NiO, and MnO_2,[8−11] and conducting redox polymers such as polyanilines, polypyrroles, and polythiophenes.[12−15] A third group of ECs are hybrid capacitors, which usually combine one battery-type faradaic electrode (as energy source) with the other capacitive electrode (as power source) in the same cell.[4] Although this type of ECs generally shows much enhanced capacitance and greatly improved energy density compared with EDLCs,[16−19] there is still a significant drawback of these hybrid capacitor devices, namely, the limited cyclability of the faradaic electrodes (considering balanced capacities for positive and negative electrodes).[20] The key to achieving high power and energy density hybrid ECs with long cycle life is to explore novel electrode material systems with rational design of material combination, morphology, and size, and proper choice of electrolytes that operate at high voltages and have excellent ionic conductivity and electrochemical stability.

To enable EC technology for large scale grid applications crucial for the future "smart" grid, which is expected to integrate a significant amount of renewable energy from solar and wind, requires the development of low-cost energy storage systems with appropriate performance characteristics.[3] There are two key aspects to meet these requirements: inexpensive yet high-performance materials with rationally designed architectures and scalable processing for low-cost fabrication. From the point of view of materials, a promising strategy would be incorporating earth-abundant capacitive carbon materials with low-cost pseudocapacitive metal oxides such as MnO_2, which offers both cost advantage and potentially high performance benefiting from both mechanisms of electric double layer capacitance and pseudocapacitance. Given that MnO_2 is one of the most promising pseudocapacitive materials due to its low cost, environmental benignity, and most importantly, high theoretical specific capacitance, there are indeed several research studies that have explored MnO_2/carbon-based composite materials for EC applications.[18,21−26] In addition, from the perspective of the fabrication process, highly scalable approaches to make functional electrodes and construct ECs, such as facile solution-based process and printing technique, will be of great importance to provide a long-term solution for making large-scale and low-cost devices. For instance, solution-based coating and printing techniques have been recently exploited by our group and others to make conductive carbon nanotubes (CNTs)-based papers and textiles as electrodes and/or current collectors for batteries and supercapacitors.[26−29] Although these CNTs-incorporated papers and textiles show exciting properties, to realize large-scale energy storage applications significant cost reduction of CNTs is still needed.

In the present work, we demonstrate a novel structure based on graphene/MnO_2 nanostructured textiles where solution-exfoliated graphene nanosheets were conformably coated on porous textile fibers, serving as conductive three-dimensional (3D) frameworks for subsequent controlled electrodeposition of MnO_2 nanomaterials. Such 3D porous networks not only permit large loading of active electrode materials but facilitate easy access of electrolytes to the electrodes. These graphene/MnO_2 composite nanostructures based energy textiles yielded greatly improved capacitive performance with specific capacitance of

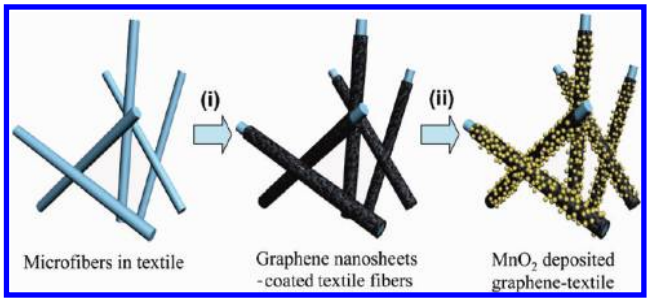

Figure 1. Schematic illustration of two key steps for preparing hybrid graphene/MnO_2-nanostructured textiles as high-performance EC electrodes. (i) Conformal coating of solution-exfoliated graphene nanosheets (gray color) onto textile fibers. (ii) Controlled electrodeposition of MnO_2 nanoparticles (yellow dots) on graphene-wrapped textile fibers.

~315 F/g achieved, which is ~5 times as high as that of energy textiles coated only with graphene nanosheets. Furthermore, high-performance hybrid ECs with graphene/MnO_2-textile as the positive electrode and SWNTs-textile as the negative electrode were fabricated and tested in aqueous 0.5 M Na_2SO_4 electrolyte. We believe that nanoscale electrode structures based on conductive, porous, 3D frameworks could provide critical breakthroughs for designing future multifunctional EC architectures. Such rationally designed ECs also exhibited significantly improved cycling performance relative to current pseudocapacitors.

Our approach for making hybrid graphene/MnO_2 nanostructures based energy textile as the EC electrode involves two key steps, as shown in Figure 1. The first is to coat highly porous textile fibers with graphene nanosheets that are prepared via a facile solution-based exfoliation process. The coating is done by a simple "dip and dry" process, similar to that widely used in the textile industry for dyeing fabrics and fibers. The second is the controlled deposition of MnO_2 nanomaterials on the as-prepared conductive textile fibers. In our study, electrochemical deposition, a proven efficient method for synthesis of a range of nanomaterials including metal, metal oxide, and conducting polymers,[30] has been used to deposit pseudocapacitive MnO_2 nanostructures in a controlled manner on graphene-wrapped conductive textiles.

Graphene materials have emerged as a unique class of carbon-based nanoscale building blocks with substantial potential for energy conversion and storage devices thanks to an array of their exceptional characteristics including superior electronic and mechanical properties, good electrochemical stability, and large specific surface area.[31] Recently, they have been explored as promising electrode materials in a variety of energy applications such as photovoltaics, batteries, and supercapacitors.[32−35] To explore tremendous potential of graphene for large scale energy storage devices, we adopted in this work a high-throughput solution-based exfoliation technique reported by Coleman et al.,[36] to prepare graphene "ink" solution (see Supporting Information). The liquid phase surfactant-assisted exfoliation in water allows the facile preparation of large-scale, homogeneous graphene dispersions of varying concentrations, showing great advantages over most other exfoliation routes that often involve the oxidation and exfoliation of powdered graphite to yield graphene oxide, and subsequent reduction steps either by high-temperature thermal annealing or chemical methods.[37] Moreover, solution-exfoliation of graphene nanosheets from graphite provides a promising low-cost approach for large-scale energy storage

dx.doi.org/10.1021/nl2013828 |Nano Lett. XXXX, XXX, 000–000

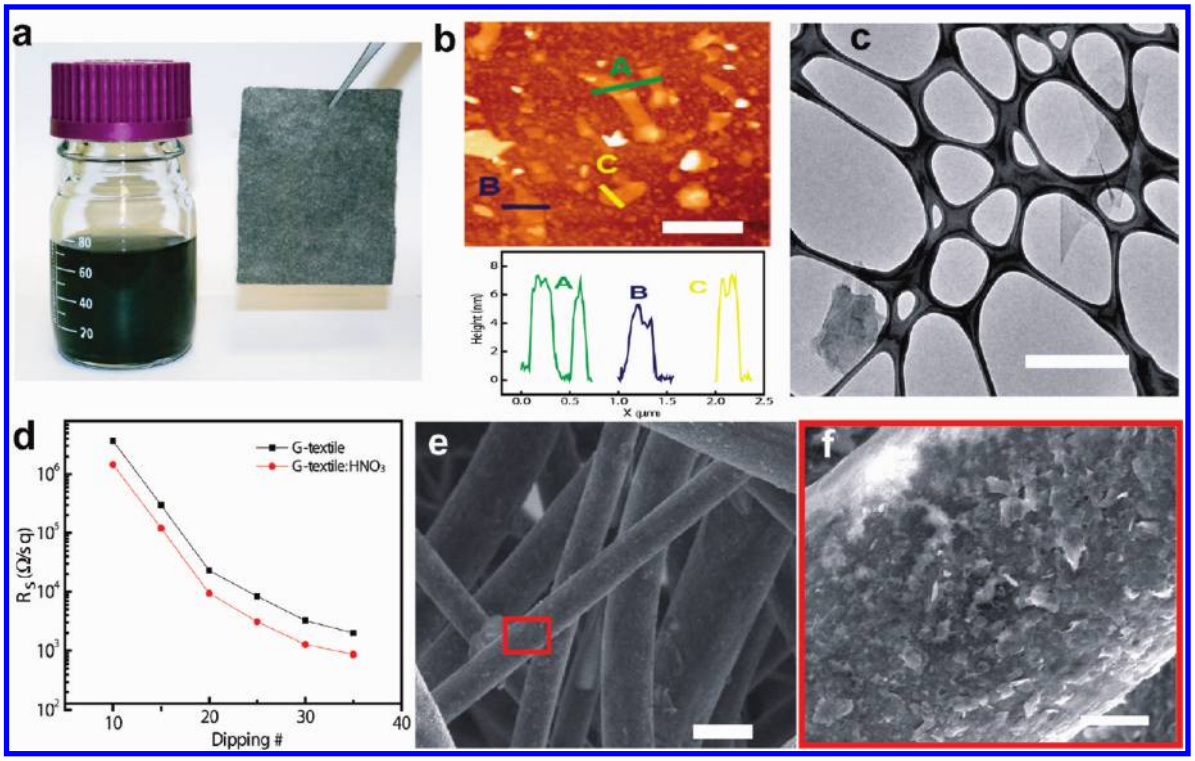

Figure 2. Coating graphene nanosheets onto porous textiles. (a) Photograph of a stable, solution-exfoliated graphene ink suspension prepared by ultrasonication of the graphite powder in a water−sodium cholate solution, and a 6 cm × 8 cm graphene-coated conductive textile sheet (polyester fabrics). (b) AFM image of solution-exfoliated graphene nanosheets deposited on a SiO_2/Si substrate and the corresponding line scan profiles for three typical graphene flakes (marked in different colors). As-produced graphene nanosheets have an average thickness of ~5 nm (multilayered graphene) and an average lateral dimension of ~0.6 μm. Scale bar: 1 μm. (c) Typical TEM image of solution-exfoliated graphene nanosheets. Scale bar: 1 μm. (d) Sheet resistances R_s versus the number of dipping cycle for graphene-coated fabric sheets (G-textile) with and without nitric acid treatment. The final graphene-wrapped textile with nitric acid treatment has a sheet resistance of ~700 Ω/sq. (e) SEM image of a sheet of graphene-coated textile showing a large-scale view of polyester fibers. Scale bar: 20 μm. (f) High-magnification SEM image (on the region highlighted in red rectangle in e) showing the uniform coating of graphene nanosheets on the surface of fabric fibers. Scale bar: 2 μm.

devices, a significant step beyond our earlier work of carbon nanotubes-based conductive textiles.[26]

We have employed the simple approach of sonicating the graphite powder in an aqueous solution containing sodium cholate, an amphiphilic molecule surfactant known to stabilize graphene sheets,[38] to yield stable dispersions of exfoliated graphene as the ink for coating on textiles (Figure 2a).[36] One of the most important features associated with this solution-phase approach is that both the degree of graphite exfoliation (graphene flake size, thickness) and the concentration of graphene dispersions can be readily controlled by adjusting several system parameters such as the initial concentrations of graphite and surfactant, sonication time, and centrifugation speed and time. For example, we used atomic force microscopy (AFM) and transmission electron microscopy (TEM) (Figure 2b,c) to investigate the exfoliation state of the graphene in these dispersions including graphene flake size and flake thickness (corresponding to number of layers per flake). We observed that the increase in initial graphite concentration leads to a higher final concentration of exfoliated-graphene but with less uniform flake size, and meanwhile the longer sonication time results in the increase in the final graphene concentration yet with the correlated decrease in flake dimensions, which is consistent with what have been found by others.[36,38,39] In order to deposit graphene layers on textiles efficiently and uniformly, an ink solution with reasonable density and uniform size of exfoliated graphene is needed. Typical graphene ink solutions we used for textile coating (see Materials and Methods in Supporting Information) yielded exfoliated graphene "nanosheets" with an average flake thickness of ~5 nm (~70% in range of 4−8 nm with ~25% of flakes <4 nm) and an average flake dimension of ~0.6 μm (~85% of flakes have size in range of 0.3−1 μm) (Supporting Information Figure S1). We note that there is still room for further optimization of graphene ink preparation by adjusting the ratio of graphite and surfactant, the sonication time and centrifugation speed/time, which could produce graphene dispersions with higher quality of exfoliation (e.g., smaller flake thickness for potentially higher active surface area); greater surface area would lead to higher electrode performance of graphene-coated textiles and final graphene/MnO_2 nanostructured textiles.

Textiles have been used as unique support materials playing a significant role in the development of wearable electronics,[40] owing to their mechanical strength and flexibility, lightweight, and modifiable surface. They usually display a hierarchical structure with complex surface morphology, functional surface groups such as hydroxyl, and high microscopic porosity. In this work, we explore textiles as porous substrate materials for energy storage devices. Polyester textiles used in our studies are composed of intertwined fabric fibers with an average microfiber diameter of ~20 μm. When the textiles are dipped into the graphene ink, they are quickly coated with graphene nanosheets because of van der Waals forces between exfoliated graphene and

dx.doi.org/10.1021/nl2013828 |*Nano Lett.* XXXX, XXX, 000–000

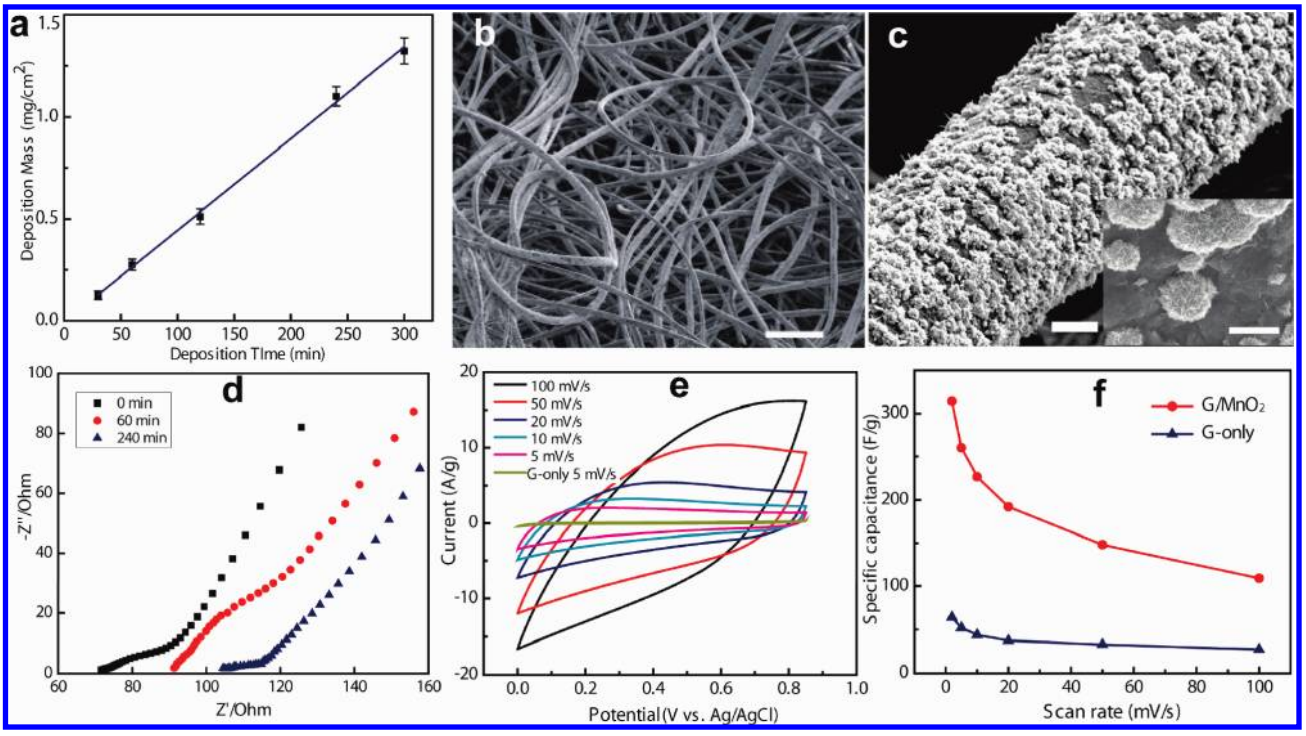

Figure 3. Energy textiles based on hybrid graphene/MnO_2 nanostructures as EC electrodes. (a) MnO_2 electrodeposition curve showing a nearly linear relationship for deposition mass versus time at an applied deposition current of 0.1 mA/cm^2. (b) SEM image of a sheet of graphene-coated textile after 60 min MnO_2 electrodeposition showing large-scale, uniform deposition of MnO_2 nanomaterials achieved on almost entire fabric fiber surfaces. Scale bar: 200 μm. (c) SEM image of a typical microfiber with conformal coating of MnO_2 nanostructures in the same textile shown in panel a. (Inset) High-magnification SEM image showing the nanoflower structure of electrodeposited MnO_2 particles and a clear interface between MnO_2 nanoflower and underneath graphene nanosheets. Scale bars are 5 and 1 μm for main figure and inset. (d) Impedance of graphene/MnO_2-textiles with different MnO_2 deposition time. Z' is real impedance and Z'' is imaginary impedance. (e) Cyclic voltammograms for graphene/MnO_2-textile electrode at different scan rates in 0.5 M aqueous Na_2SO_4 electrolyte (CV curve for graphene-only textile at a scan rate of 5 mV/s included for comparison). (f) Comparison of specific capacitance values between graphene/MnO_2-textile and graphene nanosheets-only textile at different scan rates.

polyester fibers. Subsequently, the "wet" textiles with graphene ink are subject to the drying process for water removal by putting them in an oven at 120 °C for 10 min. Through this simple dip and dry process, potentially large-area conductive graphene nanosheets-coated textiles can be readily fabricated. Figure 2d shows that the sheet resistance, R_s, decreases (conductance increases) as the dipping number in graphene ink increases. After 35 cycles, the graphene-textiles exhibit a R_s of ~700 Ω/sq. By tuning the graphene ink concentration and the dipping number, conductive textiles with a range of sheet resistance could be achieved. It should be noted that an additional step of nitric acid treatment on textiles (see Supporting Information) can help improve the conductivity by a factor of typically 2−3 compared to those without the treatment. This increase is possibly due to the effects of more thorough surfactant removal and the induced hole doping by nitric acid treatment.[41]

The representative scanning electron microscopy (SEM) image shown in Figure 2e reveals the 3D porous structures of graphene-wrapped polyester textile and demonstrates that graphene nanosheets are uniformly coated onto the microfibers over the entire sheet of fabric. A higher-magnification SEM image (Figure 2f), which almost resolves individual graphene flakes on fiber surface, confirms conformal coating of graphene nanosheets on the textile. We note that flake sizes for most graphene nanosheets (>95%) coated are in the range of 0.3−1 μm, which is in agreement with our AFM results, and those large size flakes (>2 μm, ~10% in the ink) are barely observed on the fiber surface. The conformal coating is largely due to mechanical flexibility and size uniformity of graphene nanosheets together with strong adhesion between the graphene and polyester fibers. Moreover, such porous conductive textiles conformally coated with graphene materials exhibit excellent mechanical properties and chemical resistance performance. Standard tape test and water washing on samples show little sign of graphene loss and no sheet resistance change. These tests indicate good mechanical adhesion of graphene nanosheets on textiles. Chemical resistance tests in acid (2 M sulfuric acid) and base (2 M sodium hydroxide) also show a small change in the sheet resistance (~30% increase in R_s observed for 1 h immersion for base), as found for carbon nanotubes coated textiles in previous work.[26]

Controlled deposition of nanostructured MnO_2 materials on conductive graphene-coated textiles has been achieved through an electrochemical deposition process. Graphene nanosheets conformably coated on fiber surfaces serve as a conductive support with large surface area for the subsequent deposition of nanoscale MnO_2 particles. Briefly, nitric acid-treated graphene-textiles were immersed into a plating solution containing $Mn(NO_3)_2$ and $NaNO_3$ and were subjected to electrodeposition using a three-electrode setup (see Supporting Information). The mass loading of MnO_2 can be well controlled by adjusting the deposition current and deposition time. Figure 3a shows a nearly linear relationship between deposition mass and deposition time at an applied current of 0.1 mA/cm^2, and an average deposition rate is estimated to be ~5 μg/min. Note that provided highly porous

dx.doi.org/10.1021/nl2013828 |*Nano Lett.* XXXX, XXX, 000–000

structures of polyester textiles, even larger mass loading (>3 mg/cm^2) could be achieved by increasing the deposition time to ~600 min. Considering that only a thin surface layer (often <1 μm) of MnO_2 can actively participate in pseudocapacitive reactions due to low proton diffusion constant (~ 10^{-13} cm^2/(V s)) and low electrical conductivity (~10^{-5} S/cm) of MnO_2 materials,[42] we have focused on the MnO_2 material thickness <1 μm in our studies. Figure 3b,c shows the general morphology and detailed microstructure of a typical sample prepared by 60 min deposition. We observe that uniform deposition of MnO_2 nanomaterials is achieved on the surfaces of individual microfibers over almost the entire network of porous textiles. Moreover, electrodeposited MnO_2 particles show a nanoflower-shaped hierarchical architecture with a typical dimension of 300−800 nm and hundreds of random branches forming many small mesopores of size 5−30 nm (inset, Figure 3c). The nanoflower structures observed for electrodeposited MnO_2 are consistent with other previous studies[26,43] and could provide large accessible surface areas that enable effective electrolyte ion transport during supercapacitor operations. As the electrodeposition time increases, the particle size of the nanoflower MnO_2 increases until a continuous thick film is formed on the textile fibers (Supporting Information Figure S2). Both the 3D porous structures of textiles and the good electronic conductivity of graphene layers make it possible to achieve uniform deposition and high mass loading of nanostructured MnO_2 materials with large electroactive surface areas for high performance supercapacitor electrodes.

To explore the advantages of these hybrid graphene/MnO_2 nanostructured textiles as active EC electrodes, we have investigated their electrochemical properties by performing cyclic voltammetry (CV) and electrochemical impedance spectroscopy (EIS) measurements using a three-electrode system. Figure 3d shows impedance curves of graphene/MnO_2-textile electrodes measured in a 0.5 M Na_2SO_4 electrolyte solution. The impedances at high frequency (100 kHz) reflect the equivalent series resistance (ESR) in the electrode/electrolyte system, which is contributed from both the electrolyte resistance and electronic resistance of textile electrodes. As the MnO_2 deposition time increases, the electronic resistance of the textiles increases due to the low conductivity of MnO_2 leading to an increase in ESR as seen in the figure. Figure 3e shows the rate-dependent CVs for graphene/MnO_2-textile electrodes with 60 min deposition time over a range of scan rates of 2−100 mV/s. The potential window tested is confined to a range of 0−0.85 V versus Ag/AgCl reference electrode. It can be seen that graphene/MnO_2 textile electrodes show relatively rectangular CV curves for scan rates up to 20 mV/s indicating a nearly ideal supercapacitor behavior, and at the same scan rate the resulting current from graphene/MnO_2-textile is much higher than that of graphene-only textile owing to the loading of the pseudocapacitive MnO_2. As the scan rate increases (50 and 100 mV/s), the peak current increases and the shape of CV curves shows some distortions from an ideal capacitor, possibly due to increasing overpotentials from ion transport between the electrolyte and MnO_2. Meanwhile we found that only ~40% capacitance loss when scan rate increases by a factor of 10 (5 mV/s to 50 mV/s), showing a good rate capability of graphene/MnO_2-textile electrodes. More importantly, the specific capacitance values versus scan rates based on the total mass of active electrode materials, as summarized in Figure 3f, demonstrate that our hybrid graphene/MnO_2 nanostructures based textiles yield greatly improved capacitance performance with 4−5 times increase in specific capacitance compared to that of graphene nanosheets-only textiles. The highest specific capacitance achieved is ~315 F/g at scan rate of 2 mV/s, exceeding those previously reported based on MnO_2/graphene materials system.[24,44]

Several unique characteristics of our graphene/MnO_2 nanostructured textiles make them a promising candidate for high-performance EC electrode materials. These features include the following: (i) 3D porous microstructures of the polyester textiles allowing conformal coating of graphene nanosheets and subsequent loading of MnO_2 and facilitating easy access of electrolyte ions (Na^+ in our case) to electrode surfaces; (ii) graphene nanosheets coatings serving as high surface area, conductive paths for the deposition of MnO_2 and providing excellent interfacial contact between MnO_2 and graphene for fast electron transport; and (iii) nanoflower architectures of electrodeposited MnO_2 offering large electrochemically active surface areas for charge transfer and reduced ion diffusion length during the charge/discharge process.

Asymmetric EC systems consisting of different types of electrodes have been extensively explored recently as they promise a wider operating voltage thus providing higher energy density.[9,10,18,19] We choose our graphene/MnO_2-textile as the positive electrodes and SWNT-textile as the negative electrodes to assemble hybrid ECs in 0.5 M Na_2SO_4 aqueous electrolytes, as shown in Figure 4a. The choice of SWNT-coated textiles as the negative electrodes is based on two facts: (i) that they have been demonstrated as high performance electrodes with exceptional cyclability (~2% capacitance loss over 100,000 cycles),[26] which can eliminate their contribution in capacitance loss during cycling test of our hybrid ECs, and (ii) that the operation voltages of asymmetric ECs based on MnO_2 and carbon materials can be achieved up to ~2 V in aqueous medium.[45,46] Figure 4b shows the impedance of the full cell with an ESR of ~8 Ω at high frequency of 100 kHz. Galvanostatic charging/discharging test was also performed with different current densities in a stable voltage window of 0−1.5 V, as shown in Figure 4c. The linear voltage−time profiles and the symmetric charge/discharge characteristics indicate good capacitive behavior with a rapid $I-V$ response for our asymmetric EC devices.

To evaluate further the device performance of our hybrid ECs based on graphene/MnO2-textile and CNT-textile, the energy density (E) and power density (P) were calculated from galvanostatic charge/discharge curves (for calculations see Supporting Information). The total resistance based on the internal resistance (IR) drop from the charge−discharge curves is used to calculate P and E for the assembled device, and we found these resistance values (~11−15 Ω) are relatively close to the value (~8 Ω, Figure 4b) obtained from the EIS measurement. Figure 4d shows the Ragone plot of our specific E versus P values considering the total mass of active materials from positive and negative electrodes. The maximum energy density of 12.5 Wh/kg and the highest power density of 110 kW/kg are achieved using our hybrid ECs at an operation voltage of 1.5 V. Compared to similar systems reported previously using symmetric MnO_2/MnO_2[9] or other hybrid MnO_2/carbon-based materials (CNTs, activated carbon),[18,19,46] our hybrid ECs exhibit comparable energy density but substantially higher power density. We believe that further improvement in energy density can be achieved with higher mass loading of MnO_2 nanomaterials and optimized mass balance of both electrodes for hybrid ECs to allow stable, higher voltage operation in ionic liquid electrolytes.

In addition, our high-performance hybrid ECs exhibited excellent cycling stability, which is one of the most critical factors in supercapacitor operations. MnO_2-based supercapacitors often suffer from

dx.doi.org/10.1021/nl2013828 |Nano Lett. XXXX, XXX, 000–000

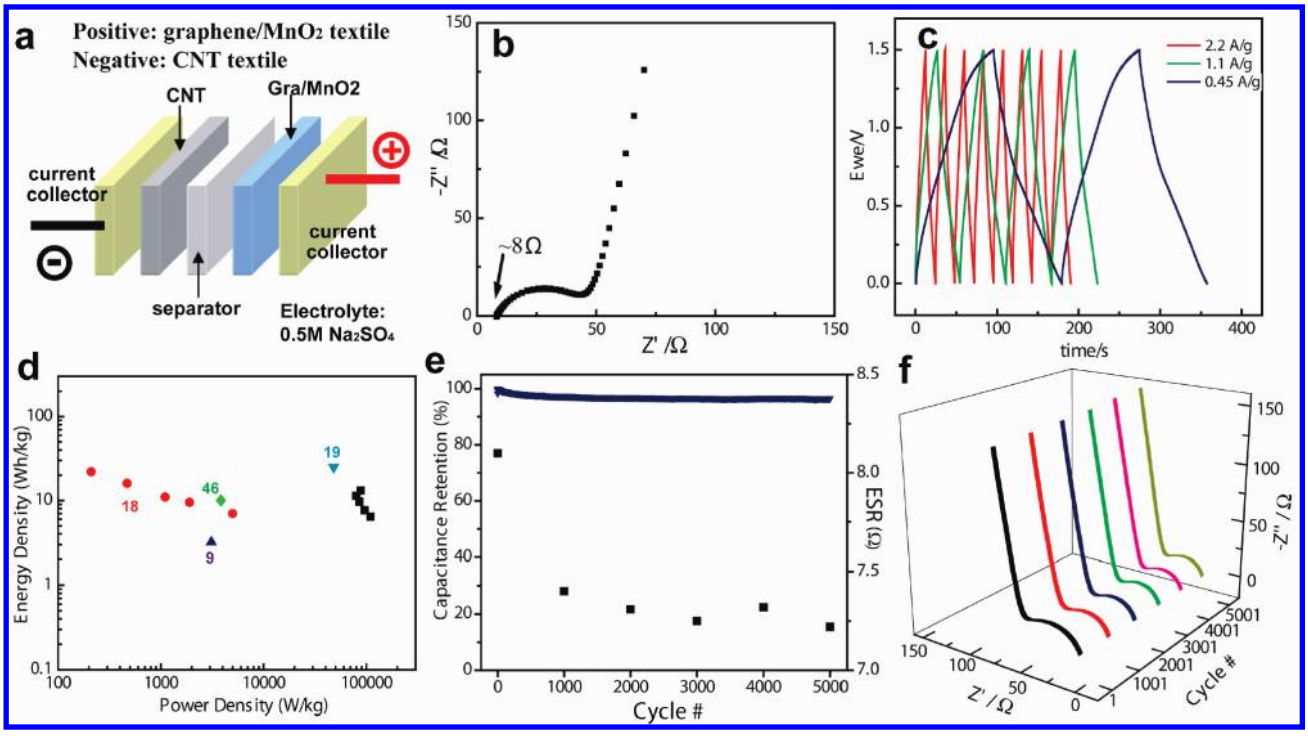

Figure 4. Asymmetric (hybrid) ECs based on graphen/MnO_2-textile as positive electrode and CNT-textile as negative electrode. (a) Schematic of the assembled structure of hybrid EC cells in a 0.5 M Na_2SO_4 aqueous electrolyte. (b) Nyquist plot for the assembled hybrid EC over the frequency range of 100 kHz ~ 0.1 Hz. Equivalent series resistance extracted is about 8 Ω. (c) Galvanostatic charging/discharging curves measured with different current densities for the assembled hybrid EC. (d) Ragone plot of energy density versus power density for our hybrid ECs (black points) and others using similar systems reported in literatures (refs 9, 18, 19, and 46). (e) Cycling performance of our hybrid ECs showing capacitance retention of ~95% after 5000 cycles of charging and discharging at a current density of 2.2 A/g, and subtle change in EC's equivalent series resistance taken from impedance measurement every 1000 cycles. (f) Nyquist plots showing the corresponding impedance curves measured after each 1000 cycles during cycling test for assembled ECs.

limited cyclability due to some of the following issues: mechanical expansion of MnO_2 during ion insertion/desertion process, MnO_2 film detachment from electrode surfaces, Mn dissolution into electrolyte, and imbalanced capacity on two electrodes causing the instability of the electrode potential.[20] In contrast, the cycling test of our hybrid EC cells shows ~95% capacitance retention over 5000 cycles at a high current density of 2.2 A/g, which is significantly better than those reported in previous work (typically 70−85% retention over 1000 cycles).[18,24,45] EIS measurements after each 1000 cycles demonstrate a subtle change in ESR over the entire 5000 cycles and Nyquist plots of experimental impedance data show the consistent impedance spectra, further demonstrating exceptional electrochemical stability of the hybrid ECs. The excellent cycling performance achieved in our EC system can be attributed to a number of factors. Besides the key advantages aforementioned for this unique electrode architecture, excellent interfacial contact between MnO_2 nanostructures and graphene layers that likely resulted from hydrogen bonding between MnO_2 and carboxylated edge surface of graphene may be another important enabling factor. In fact, we characterized the morphology and structure of our graphene/MnO_2-textile electrodes after 5000 cycles, and found that the nanoflower MnO_2 structures were well maintained and the MnO_2 was still uniformly coated on textile fibers (Supporting Information Figure S3).

In summary, we have developed a scalable solution-based approach to fabricate hybrid graphene/MnO_2 nanostructured textiles as high-performance supercapacitor electrodes. The unique architecture of these designed textiles allows efficient use of pseudocapacitive MnO_2 nanomaterials for charge storage with facilitated transport of both electrolyte ions and electrons, thus rendering the composite materials with high specific capacitance, good rate capability and remarkable cycling performance. We believe that such low-cost, lightweight, and high-performance energy textiles realized by earth-abundant and environment-friendly materials and scalable solution processing, can offer great promise in grid-scale energy storage device applications.

■ ASSOCIATED CONTENT

Supporting Information. Materials and Methods and additional supporting figures. This material is available free of charge via the Internet at http://pubs.acs.org.

■ AUTHOR INFORMATION

Corresponding Author

*E-mail: (Y.C.) yicui@stanford.edu; (Z.B.) zbao@stanford.edu.

Author Contributions

¶These authors contributed equally.

■ ACKNOWLEDGMENT

We thank Dr. Yan Yao and Dr. Hanying Li for their helpful discussion and assistance in some sample characterizations. Y.C. and Z.B. acknowledge the funding support from the Precourt

Institute for Energy at Stanford University. Y.C. also acknowledges the funding support from the King Abdullah University of Science and Technology (KAUST) Investigator Award (No. KUS-l1-001-12). X.C. acknowledges the support from Stanford Undergraduate Research Experience Program.

REFERENCES

(1) Burke, A. *J. Power Sources* **2000**, *91*, 37.
(2) Conway, B. E. *J. Electrochem. Soc.* **1991**, *138*, 1539.
(3) Yang, Z.; Zhang, J.; Kintner-Meyer, M. C. W.; Lu, X.; Choi, D.; Lemmon, J. P.; Liu, J. *Chem. Rev.* **2011**, *111* (5), 3577–3613.
(4) Simon, P.; Gogotsi, Y. *Nat. Mater.* **2008**, *7*, 845.
(5) Miller, J. R.; Simon, P. *Science* **2008**, *321*, 651.
(6) Conway, B. E. *Electrochemical Supercapacitors:Scientific Fundamentals and Technological Applications*; Kluwer Academic/Plenum: New York, 1999.
(7) Huang, J.; Sumpter, B. G.; Meunier, V. *Angew. Chem., Int. Ed.* **2008**, *47*, 520.
(8) Brousse, T.; Toupin, M.; Dugas, R.; Athouel, L.; Crosnier, O.; Belanger, D. *J. Electrochem. Soc.* **2006**, *153*, A2171.
(9) Cottineau, T.; Toupin, M.; Delahaye, T.; Brousse, T.; Bélanger, D. *Appl. Phys. A* **2006**, *82*, 599.
(10) Wang, D.-W.; Li, F.; Cheng, H.-M. *J. Power Sources* **2008**, *185*, 1563.
(11) Wu, N.-L. *Mater. Chem. Phys.* **2002**, *75*, 6.
(12) Rudge, A.; Davey, J.; Raistrick, I.; Gottesfeld, S.; Ferraris, J. *J. Power Sources* **1994**, *47*, 89.
(13) Fusalba, F.; Gouerec, P.; Villers, D.; Belanger, D. *J. Electrochem. Soc.* **2001**, *148*, A1.
(14) Frackowiak, E.; Khomenko, V.; Jurewicz, K.; Lota, K.; Béguin, F. *J. Power Sources* **2006**, *153*, 413.
(15) Mastragostino, M.; Arbizzani, C.; Soavi, F. *J. Power Sources* **2001**, *97−98*, 812.
(16) Min, M.; Machida, K.; Jang, J. H.; Naoi, K. *J. Electrochem. Soc.* **2006**, *153*, A334.
(17) Sivakkumar, S. R.; Kim, W. J.; Choi, J.-A.; MacFarlane, D. R.; Forsyth, M.; Kim, D.-W. *J. Power Sources* **2007**, *171*, 1062.
(18) Wu, Z.-S.; Ren, W.; Wang, D.-W.; Li, F.; Liu, B.; Cheng, H.-M. *ACS Nano* **2010**, *4*, 5835.
(19) Chen, P.-C.; Shen, G.; Shi, Y.; Chen, H.; Zhou, C. *ACS Nano* **2010**, *4*, 4403.
(20) Naoi, K.; Simon, P. *Electrochem. Soc. Interface* **2008**, *17*, 34.
(21) Chang, J.-K.; Lin, C.-T.; Tsai, W.-T. *Electrochem. Commun.* **2004**, *6*, 666.
(22) Sivakkumar, S. R.; Ko, J. M.; Kim, D. Y.; Kim, B. C.; Wallace, G. G. *Electrochim. Acta* **2007**, *52*, 7377.
(23) Ma, S.-B.; Nam, K.-W.; Yoon, W.-S.; Yang, X.-Q.; Ahn, K.-Y.; Oh, K.-H.; Kim, K.-B. *J. Power Sources* **2008**, *178*, 483.
(24) Chen, S.; Zhu, J.; Wu, X.; Han, Q.; Wang, X. *ACS Nano* **2010**, *4*, 2822.
(25) Lee, S. W.; Kim, J.; Chen, S.; Hammond, P. T.; Shao-Horn, Y. *ACS Nano* **2010**, *4*, 3889.
(26) Hu, L.; Pasta, M.; Mantia, F. L.; Cui, L.; Jeong, S.; Deshazer, H. D.; Choi, J. W.; Han, S. M.; Cui, Y. *Nano Lett.* **2010**, *10*, 708.
(27) Hu, L.; Choi, J. W.; Yang, Y.; Jeong, S.; La Mantia, F.; Cui, L.-F.; Cui, Y. *Proc. Natl. Acad. Sci. U.S.A.* **2009**, *106*, 21490.
(28) Pushparaj, V. L.; Shaijumon, M. M.; Kumar, A.; Murugesan, S.; Ci, L.; Vajtai, R.; Linhardt, R. J.; Nalamasu, O.; Ajayan, P. M. *Proc. Natl. Acad. Sci. U.S.A.* **2007**, *104*, 13574.
(29) Pasta, M.; La Mantia, F.; Hu, L.; Deshazer, H.; Cui, Y. *Nano Res.* **2010**, *3*, 452.
(30) Hodes, G. *Electrochemistry of Nanomaterials*; Wiley-VCH: Weinheim, 2001.
(31) Geim, A. K.; Novoselov, K. S. *Nat. Mater.* **2007**, *6*, 183.
(32) Kim, K. S.; Zhao, Y.; Jang, H.; Lee, S. Y.; Kim, J. M.; Kim, K. S.; Ahn, J.-H.; Kim, P.; Choi, J.-Y.; Hong, B. H. *Nature* **2009**, *457*, 706.
(33) Liang, M.; Zhi, L. *J. Mater. Chem.* **2009**, *19*, 5871.
(34) Stoller, M. D.; Park, S.; Zhu, Y.; An, J.; Ruoff, R. S. *Nano Lett.* **2008**, *8*, 3498.
(35) Zhang, L. L.; Zhou, R.; Zhao, X. S. *J. Mater. Chem.* **2010**, *20*, 5983.
(36) Lotya, M.; King, P. J.; Khan, U.; De, S.; Coleman, J. N. *ACS Nano* **2010**, *4*, 3155.
(37) Zhu, Y.; Murali, S.; Cai, W.; Li, X.; Suk, J. W.; Potts, J. R.; Ruoff, R. S. *Adv. Mater.* **2010**, *22*, 3906.
(38) Green, A. A.; Hersam, M. C. *Nano Lett.* **2009**, *9*, 4031.
(39) Lotya, M.; Hernandez, Y.; King, P. J.; Smith, R. J.; Nicolosi, V.; Karlsson, L. S.; Blighe, F. M.; De, S.; Wang, Z.; McGovern, I. T.; Duesberg, G. S.; Coleman, J. N. *J. Am. Chem. Soc.* **2009**, *131*, 3611.
(40) Park, S.; Jayaraman, S. *MRS Bull.* **2003**, *28*, 585.
(41) Kasry, A.; Kuroda, M. A.; Martyna, G. J.; Tulevski, G. S.; Bol, A. A. *ACS Nano* **2010**, *4*, 3839.
(42) Bélanger, D.; Brousse, T.; Long, J. W. *Electrochem. Soc. Interface* **2008**, *17*, 49.
(43) Chou, S.-L.; Wang, J.-Z.; Chew, S.-Y.; Liu, H.-K.; Dou, S.-X. *Electrochem. Commun.* **2008**, *10*, 1724.
(44) Yan, J.; Fan, Z.; Wei, T.; Qian, W.; Zhang, M.; Wei, F. *Carbon* **2010**, *48*, 3825.
(45) Khomenko, V.; Raymundo-Piñero, E.; Béguin, F. *J. Power Sources* **2006**, *153*, 183.
(46) Brousse, T.; Toupin, M.; Belanger, D. *J. Electrochem. Soc.* **2004**, *151*, A614.